Letter

Superkicks and the photon angular and linear momentum density

Andrei Afanasev,[1] Carl E. Carlson,[2] and Asmita Mukherjee[3]
[1]*Department of Physics, George Washington University, Washington, DC 20052, USA*
[2]*Physics Department, William & Mary, Williamsburg, Virginia 23187, USA*
[3]*Department of Physics, Indian Institute of Technology Bombay, Powai, Mumbai 400076, India*

(Received 24 February 2022; revised 3 June 2022; accepted 8 June 2022; published 27 June 2022)

We address the problem of determining the physically correct definition of the momentum and angular momentum densities in a spatially structured electromagnetic field, given that the expressions are not the same when one uses the canonical energy-momentum tensor instead of the symmetric Belinfante energy-momentum tensor in electrodynamics. This has important consequences for the interaction of matter with structured light, for example, twisted photons, and would give drastically different results for forces and angular momenta induced on small test objects. We show, with numerical estimates of the size of the effects, situations where the canonical and symmetrized forms induce very different torques or (superkick) recoil momenta on small objects or atomic rotors, over a broad range of circumstances.

DOI: 10.1103/PhysRevA.105.L061503

Introduction. Disagreement over the correct expression for the linear or angular momentum density of electromagnetic beams remains. Light beams with nontrivial wave fronts—structured light—in particular twisted-photon beams, give an opportunity both for adjudicating the controversy and for dramatic results whatever the outcome.

Twisted photons are vortexlike solutions to the Helmholtz equation in cylindrical coordinates which have fields swirling around a vortex line, whose angular momentum in the direction of propagation m_γ is any integer times $\hbar$. They stand in stark contrast to plane-wave photons where $m_\gamma = \pm\hbar$ only. For reviews, see [1,2], and for further discussions of momentum definitions, see [2–9].

Experimentally, the large total angular momentum is verified. For example, in [10,11], where twisted photons were absorbed by small objects suspended in a viscous fluid, the objects were observed to acquire spins in agreement with the heightened angular momentum of the twisted photon. However, in these experiments the objects, although small, are large enough to absorb the entire twisted beam and so measured total angular momentum and not the local angular momentum density of the beam.

Quantum-state control of trapped ions using laser beams is presently one of the most promising techniques for quantum computing [12]. The spatial extent of the ion's wave function in a harmonic oscillator trap may be, for example, about 5 nm [13] if the ion is cooled close to the oscillator's ground state. With such localization of the objects compared to the micron wavelength of light used to manipulate them, the question of how one should calculate the linear and angular momentum density of the electromagnetic field becomes important. There is a canonical procedure that leads to a certain expression, reviewed below, that can, in turn, be obtained from a canonical expression for the energy-momentum tensor that is not symmetric in its two indices. Citing both aesthetics and needs of general relativity, one can add a total derivative to make the energy-momentum tensor symmetric, a procedure pioneered by Belinfante [14] and by Rosenfeld [15], and then obtain a different expression for the angular momentum density, also reviewed below. Because of the total derivative, the integrals that give the total angular momentum are identical if the surface terms cause no problem.

However, as emphasized particularly in [16,17], when structured light shines on rings or, generally, on small objects with open centers, the angular momentum absorbed or the torque induced depends on the angular momentum density expressions at radii where the matter exists, and the expressions are rather different for the canonical and symmetrized or Belinfante cases. Further, Ref. [6] suggests an alternative geometric spin Hall effect in light, where the canonical and Belinfante predictions are quite distinct, so that measurements could show that either or both of them must be wrong. Reference [7] showed that one could obtain the same momentum in a confined volume using the canonical density as the one that would be gotten using the Belinfante density if one accounted for the surface terms but did not, to our minds, argue decisively which density was physically correct. References [8,9] reported measurements of transverse optical forces on small particles in Bessel beams, but at selected locations where the canonical and Belinfante force predictions happened to be the same. We will comment on further opportunities with this type of measurement in the text below.

Alternatively, one may discuss the effect of twisted light on small objects in terms of superkicks, to use a term coined in [18], to describe the effects of the sometimes quite large azimuthal components of the linear momentum density. Specific examples of superkicks and possibilities to observe this quantum effect were recently considered in Refs. [19,20]. The calculated size of the superkick depends critically upon whether one uses the canonical or Belinfante expression.

Close to the vortex line, the canonically calculated superkick is much larger, and farther out there are broad regions where superkicks differ in sign.

There is a separate discussion, which we will not enter into, in both the canonical and symmetrized contexts of how to write the angular momenta for the fermions and vector bosons in QED or QCD, with distinct spin and orbital angular momenta for each field, while maintaining gauge invariance. For a review of this discussion, see [21].

The goal of this Letter is to show examples, with numerical estimates, for the forces, torques, and accelerations in situations where the canonical and Belinfante forms of the linear or angular momentum density lead to very different results. We will begin with a short review, followed by studies of twisted photons axially striking hollow cylinders, of twisted photons impinging on and accelerating a two-ion rotor, of small particles struck while off axis in a twisted beam, and of radiation pressure on small objects appearing as tractor beams in limited regions.

A brief review of the formalism. The electromagnetic Lagrangian is $L = -F_{\alpha\beta}F^{\alpha\beta}/(4\mu_0)$. Studying the response of the Lagrangian to coordinate translations leads to a canonical and conserved (in the first index) energy-momentum tensor (see, e.g., [22,23])

$$T^{\mu\nu} = -\frac{1}{\mu_0}F^{\mu\alpha}\partial^\nu A_\alpha - g^{\mu\nu}L. \tag{1}$$

The tensor is not symmetric. It can be made symmetric by adding a total derivative $-\partial_\alpha(F^{\mu\alpha}A^\nu)/\mu_0$, which by virtue of the equations of motion leads to a symmetric, or Belinfante, energy-momentum tensor

$$\theta^{\mu\nu} = -\frac{1}{\mu_0}F^{\mu\alpha}F^\nu_{\ \alpha} - g^{\mu\nu}L. \tag{2}$$

The tensor remains conserved.

The linear momentum densities $\mathcal{P}^\nu$ are the $T^{0\nu}/c$ or $\theta^{0\nu}/c$ components of these tensors, so that

$$\vec{\mathcal{P}} = \begin{cases} \epsilon_0\vec{E}\cdot(\vec{\nabla})\vec{A}, & \text{canonical,} \\ \epsilon_0\vec{E}\times\vec{B}, & \text{symmetric, or Belinfante.} \end{cases} \tag{3}$$

The last is also the Poynting vector times $1/c^2$, and the notation in the first line means $\mathcal{P}^i_{\rm can} = \epsilon_0\sum_{j=1}^3 E^j\nabla_i A^j$.

Further, Lorentz and rotation transformations lead to a canonical angular momentum tensor

$$\mathcal{M}^{\alpha\mu\nu} = x^\mu T^{\alpha\nu} - x^\nu T^{\alpha\mu} + \frac{\partial L}{\partial(\partial_\alpha A_\beta)}\Sigma^{\mu\nu}_{\beta\gamma}A^\gamma, \tag{4}$$

with $\Sigma^{\mu\nu}_{\beta\gamma} = g^\mu_\beta g^\nu_\gamma - g^\mu_\gamma g^\nu_\beta$. The canonical angular momentum densities $\vec{\mathcal{J}}$ come from $\mathcal{M}^{0ij}/c$. For the symmetrical, or Belinfante, case, one just takes $\vec{r}$ times the corresponding momentum density, with no explicit spin term.

$$\vec{\mathcal{J}} = \begin{cases} \epsilon_0\vec{E}\cdot(\vec{r}\times\vec{\nabla})\vec{A} + \epsilon_0\vec{E}\times\vec{A}, & \text{canonical,} \\ \epsilon_0\,\vec{r}\times(\vec{E}\times\vec{B}), & \text{symmetrical, or Belinfante.} \end{cases} \tag{5}$$

The two expressions differ by a total derivative. But they differ locally, so they do not lead to the same torque upon small test objects.

For the $\mathcal{J}_z$ components, the differences when considering structured light are large and robust. As the discussion proceeds, we will begin with these components.

In the paraxial approximation, the transverse part of the vector potential is

$$\vec{A}(\vec{r},t) = \hat{\epsilon}\,u(\rho,\phi,z)e^{i(kz-\omega t)}. \tag{6}$$

Here ρ, ϕ, and z are cylindrical coordinates; z is the overall propagation direction of the beam, and $\hat{\epsilon}$ is a polarization vector,

$$\hat{\epsilon} = a\hat{\eta}_+ + b\hat{\eta}_-, \tag{7}$$

with $\eta_\Lambda = (-\Lambda\hat{x} - i\hat{y})/\sqrt{2}$ and $|a|^2 + |b|^2 = 1$, with $\Lambda = \pm 1$. Also we will let $\sigma_z \equiv |a|^2 - |b|^2$. Using angle brackets to denote the time average, the z components of the angular momentum densities are

$$\begin{aligned} \langle\mathcal{J}_z\rangle_{\rm can} &= \left(\frac{1}{2}\epsilon_0\omega\right)(\ell+\sigma_z)|u|^2, \\ \langle\mathcal{J}_z\rangle_{\rm Bel} &= \left(\frac{1}{2}\epsilon_0\omega\right)\left[(\ell+\sigma_z)|u|^2 - \frac{\sigma_z}{2\rho}\frac{\partial(\rho^2|u|^2)}{\partial\rho}\right]. \end{aligned} \tag{8}$$

The total angular momentum along the beam direction is $m_\gamma\hbar = (\ell+\sigma_z)\hbar$, on a per photon basis.

We will work with Bessel-Gauss solutions for the function u; the results are similar to Laguerre-Gauss beams for suitable choices of parameters. For the Bessel-Gauss beams

$$u(\rho,\phi,z) = u(\rho,\phi) = A_0 J_\ell(\kappa\rho)e^{i\ell\phi}e^{-\rho^2/w_0^2}. \tag{9}$$

The monochromatic angular frequency is ω; $k = \omega/c$; $\kappa = k\sin\theta_k$, with θ_k being the pitch angle whose smallness defines the paraxial approximation; and J_ℓ is a Bessel function. The Gaussian width of the envelope is w_0.

Plots of these densities as a function of distance from the vortex line, given in terms of the wavelength λ, are shown in Fig. 1 for total angular momenta $m_\gamma = 1$ and 2, $\theta_k = 0.1$, polarization $\sigma_z = 1$, selected pitch angle, and Gaussian envelope width $w_0 = 10\lambda$. The canonical angular momentum density is never negative (and with no paraxial approximation is never zero except at $\rho = 0$). However, the symmetric, or Belinfante, case has regions where the angular momentum density swirls in a direction opposite the overall angular momentum. These remarkable opposite-swirling regions are broad, and the predictions of their location and strength are not sensitive to making or not making the paraxial or other approximations.

Twisted photons incident on a hollow cylinder. To see what torques and angular velocities might be imparted to real test objects, we consider a specific measurement situation. We think of the twisted photon shining on a ring or in three dimensions a test object which is a hollow cylinder with its axis identical to the vortex axis of the twisted-photon beam, as depicted in Fig. 2(a). We will suppose that all the light, and the angular momentum it contains, hitting the front edge of the cylinder is absorbed by the cylinder. We calculate first the angular acceleration the cylinder would have if it were in free space, and then we calculate the terminal angular velocity it would obtain if it were suspended in a viscous fluid.

If the hollow cylinder has an average radius ρ with inner and outer radii $\rho \pm (1/2)\Delta\rho$, then the torque from absorbing

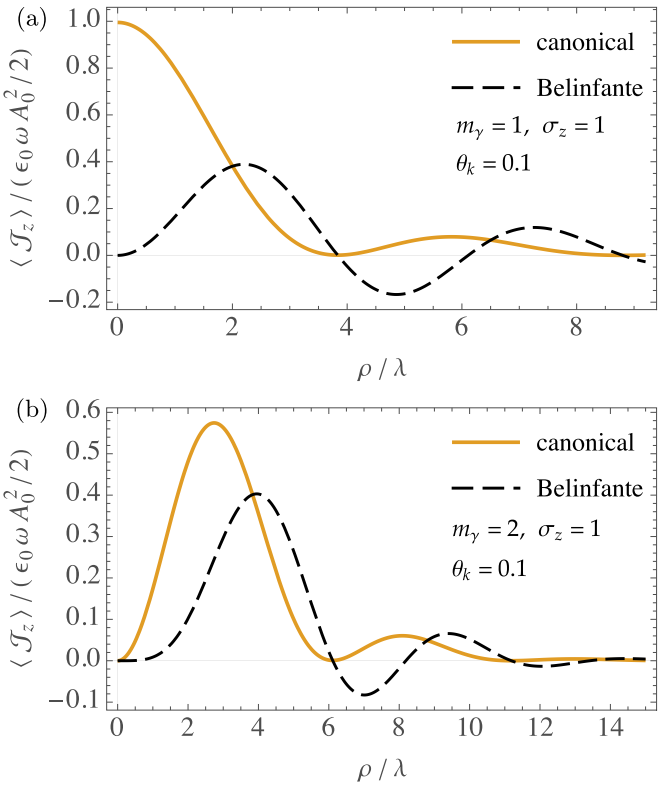

FIG. 1. Angular momentum density on a ring of radius ρ for a twisted light beam of (a) total angular momentum $m_\gamma = 1$ and (b) $m_\gamma = 2$ and circular polarization $\sigma_z = 1$, with angular frequency ω and A_0 normalizing the strength of the beam's electric field. The Belinfante case has regions where the angular momentum density swirls in a direction opposite the overall angular momentum.

the light on the front face of area σ is

$$\langle \tau_z \rangle = \sigma c \, \langle \mathcal{J}_z \rangle = (2\pi \rho \Delta \rho) c \, \langle \mathcal{J}_z \rangle \, . \tag{10}$$

We obtain the normalization A_0 from the total power in the Bessel-Gauss beam, which we get by integrating the z component of the Poynting vector. (The latter gives the energy flux whether we use the canonical or Belinfante energy-momentum tensor.) The z component of the Poynting vector

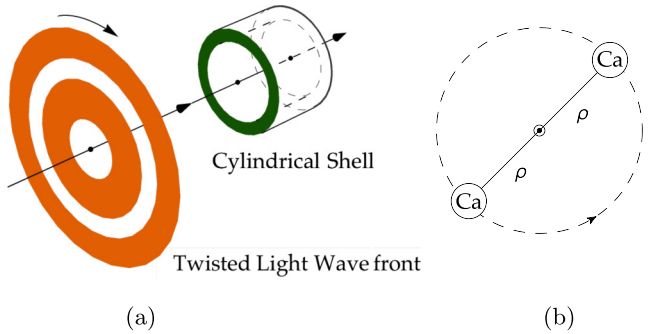

FIG. 2. (a) Twisted light hitting a hollow cylinder, with axes coincident. (b) A two-ion calcium rotor.

becomes, paraxially,

$$\langle S_z \rangle = \frac{\omega k A_0^2}{2\mu_0} J^2_{m_\gamma - \Lambda}(\kappa \rho) \, \exp\left(-2\rho^2/w_0^2\right) \tag{11}$$

for a polarized situation where $\sigma_z = \pm 1 = \Lambda$. The beam's time average power is $\langle P \rangle$, and we obtain the normalization A_0 from

$$\langle P \rangle = \int_0^\infty \langle S_z \rangle \, 2\pi \rho d\rho. \tag{12}$$

We use $\langle P \rangle = 4\,\mathrm{mW}$, wavelength $\lambda = 729\,\mathrm{nm}$, and $w_0 = 10\lambda$. The latter two numbers match conditions in [13,24], and the first matches the quoted power of a twisted beam delivered on a target in [10]. For definiteness, we consider the $m_\gamma = 2$ case, wall thickness $\Delta\rho = 0.5\,\mu$m, and length $L = 2\,\mu$m. We will give explicit numbers for $\rho = 2\,\mu$m, a value of ρ near the peak of the angular momentum density for the $m_\gamma = 2$ canonical case [see Fig 1(b)]. Results for other values of ρ can be scaled from the results in Fig. 1.

The moment of inertia is $I = M\rho^2 = 2\pi \rho_m \rho^3 \Delta\rho L$, where M is the mass of the cylindrical shell and ρ_m is its mass density, which for the sake of illustration we take as two times the density of water. The angular acceleration $\langle \alpha \rangle = \langle \tau_z \rangle / I$ for the cylinder in free space is

$$\langle \alpha \rangle \approx \begin{cases} 5.5 \times 10^6\,\mathrm{rad/s^2} & \text{canonical,} \\ 2.3 \times 10^6\,\mathrm{rad/s^2} & \text{Belinfante,} \end{cases} \tag{13}$$

where τ_z is given in terms of J_z in Eq. (10).

If the cylinder is in a viscous medium, there is a drag torque on it, $\tau_{\mathrm{drag}} = -4\pi\eta\rho^2\ell\,\Omega$, where η is the viscosity and Ω is the cylinder's angular rotation frequency. If the medium is kerosine ($\eta = 1.64 \times 10^{-3}\,\mathrm{N\,s/m^2}$), the terminal rotation frequency is

$$f \approx \begin{cases} 0.55\,\mathrm{Hz} & \text{canonical,} \\ 0.23\,\mathrm{Hz} & \text{Belinfante.} \end{cases} \tag{14}$$

Again, this is the prediction for one radius. Using other radii will give different results following Fig. 1. Note that the 0.5-μm-shell thickness is narrow enough to fit within the negative region of the Belinfante curves in that Fig. 1.

A two-ion rotor. Another situation distinguishing the canonical and Belinfante calculations is twisted photons striking a two-ion rotor. Our discussion is inspired by the working rotor described in [25].

We shall describe the mechanism in term of superkicks. These come from the azimuthal component of the momentum density, which paraxially is

$$\begin{aligned} \langle \mathcal{P}_\phi \rangle_{\mathrm{can}} &= \frac{\epsilon_0 \omega A_0^2}{2\rho}(m_\gamma - \Lambda) J^2_{m_\gamma - \Lambda}(\kappa\rho), \\ \langle \mathcal{P}_\phi \rangle_{\mathrm{Bel}} &= \frac{\epsilon_0 \omega A_0^2}{2} \kappa \, J_{m_\gamma}(\kappa\rho) J_{m_\gamma - \Lambda}(\kappa\rho). \end{aligned} \tag{15}$$

The photon number density in either case is

$$\langle n_\gamma \rangle = \frac{\epsilon_0 \omega A_0^2}{2\hbar} J^2_{m_\gamma - \Lambda}(\kappa\rho). \tag{16}$$

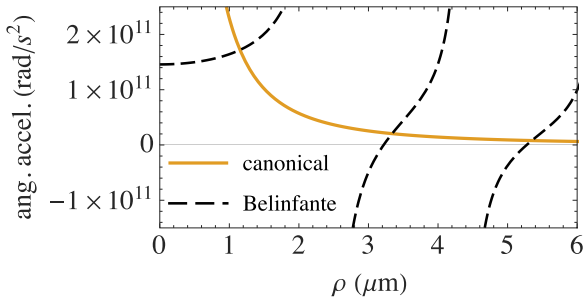

FIG. 3. Calculated angular acceleration for a two-ion calcium rotor of varying radii, with further description given in the text

The transverse momentum kick or superkick at distance ρ from the vortex line is then

$$\langle p_\phi \rangle = \frac{\langle \mathcal{P}_\phi \rangle}{\langle n_\gamma \rangle} = \begin{cases} \frac{(m_\gamma - \Lambda)\hbar}{\rho} \equiv \frac{\ell\hbar}{\rho} & \text{canonical,} \\ \hbar\kappa \frac{J_{m_\gamma}(\kappa\rho)}{J_{m_\gamma - \Lambda}(\kappa\rho)} & \text{Belinfante.} \end{cases} \tag{17}$$

For a rotor with two $^{40}Ca^+$ ions [Fig. 2(b)], we choose an atomic transition such as $4s_{1/2} \to 4p_{3/2}$ or $4p_{1/2}$, where the excited state is not metastable but has a fast spontaneous decay. The situation is analogous to laser cooling [26]: The spontaneous decay is isotropic, so statistically, there is no momentum kick in the decay, but the excitation always involves a momentum kick in the same azimuthal direction. We shine the twisted-photon beam so that its vortex line is perpendicular to the plane of the rotor and passes through its center. If the exciting laser is strong enough to quickly excite the ground-state ion, the ion will receive one momentum kick per lifetime of the excited state T. This will give a force dp/dt, a torque τ, and for moment of inertia I an angular acceleration

$$\alpha = \frac{\tau}{I} = \frac{2\rho \langle p_\phi \rangle / T}{2M\rho^2} = \frac{\langle p_\phi \rangle}{M\rho T}, \tag{18}$$

where M is the mass of the calcium ion. The lifetimes are $T(Ca^+, 4p_{3/2}) = 6.924(0.019)$ ns and $T(Ca^+, 4p_{1/2}) = 7.098(0.020)$ ns [27].

Figure 3 shows a plot of the angular acceleration vs rotor radius for the $4p_{3/2}$ case; the $4p_{1/2}$ case is barely different.

Small particles off axis in a twisted beam. References [8,9] report measurements of the azimuthal kick received by small particles sitting at various distances or various impact parameters from the vortex line of a twisted-photon beam. (The azimuthal kick is given in terms of $\Omega_{\text{revolution}}$ in, say, Fig. 2(b) of [9].) The size of the kicks, given in terms of the azimuthal or transverse component of the momentum density, is

$$p_\phi = \begin{cases} \epsilon_0 \left[\frac{\omega\ell}{\rho} |u|^2 - \frac{1}{2}\omega\sigma \frac{\partial |u|^2}{\partial \rho} \right] & \text{Belinfante,} \\ \frac{\epsilon_0 \omega \ell}{\rho} |u|^2 & \text{canonical.} \end{cases} \tag{19}$$

The Belinfante expression is also given in the middle line of Eq. (2) of [9]; the canonical expression differs in the absence of the derivative term. The measurements reported were made at the peaks of the intensity distribution in the rings of the twisted-beam wave front. The intensity distribution is proportional to $|u|^2$, so these are precisely the locations where the Belinfante and canonical predictions are the same.

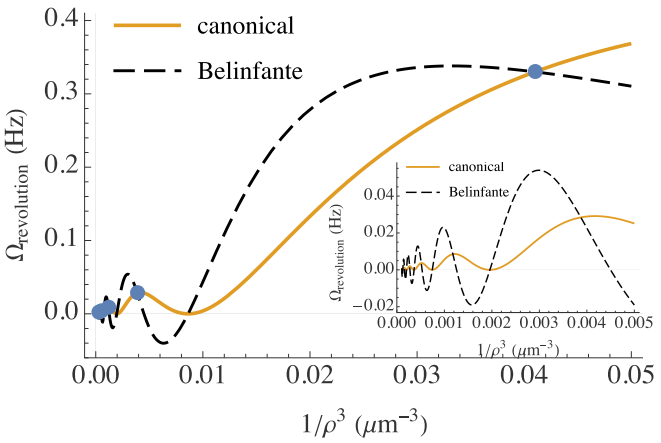

FIG. 4. Azimuthal kick given in terms of $\Omega_{\text{revolution}}$ vs radius given as $1/\rho^3$ for a small particle in a twisted electromagnetic beam. Dots indicate where current measurements lie [9].

Figure 4 shows how the expectations from the two cases differ. The vertical axis shows the revolution frequency as a small particle at radius ρ is kicked in a circular path about the vortex line. The normalization depends on the power in the beam and is chosen to match one of the power settings in Fig. 2(b) of [9]. The dots show the locations of the current measurements.

It would be worth having measurements at other radii. The zeros of intensity coincide with the zeros of canonical $\Omega_{\text{revolution}}$, so there are regions of good intensity where the canonical and Belinfante predictions differ significantly.

Radiation pressure from structured light. Let us turn now to discussing the longitudinal component of the linear momentum density and the radiation pressure forces engendered by that component. The differences between the canonical and Belinfante predictions can be dramatic. However, the dramatic differences are only in narrow regions and are sensitive to detail. We will here work with exact Bessel beam expressions. We also omit for now the Gaussian or other envelope. The Bessel beam is built from photons that all have the same longitudinal momentum and same transverse momentum magnitude but varying azimuthal angles. For the case where all the component photons have helicity Λ, the vector potential is [28–30]

$$\begin{aligned} &A^\mu_{\kappa m_\gamma k_z \Lambda}(\rho, \phi, z) \\ &= -i\Lambda A\, e^{i(k_z z - \omega t + m_\gamma \phi)} \Big\{ e^{-i\Lambda\phi} \cos^2 \frac{\theta_k}{2} J_{m_\gamma - \Lambda}(\kappa\rho)\, \eta^\mu_\Lambda \\ &\quad + \frac{i}{\sqrt{2}} \sin\theta_k J_{m_\gamma}(\kappa\rho)\, \eta^\mu_0 - e^{i\Lambda\phi} \sin^2 \frac{\theta_k}{2} J_{m_\gamma + \Lambda}(\kappa\rho)\, \eta^\mu_{-\Lambda} \Big\}, \end{aligned} \tag{20}$$

where $k_z = k\cos\theta_k$ and $\kappa = k\sin\theta_k$.

The longitudinal components of the momentum density are

$$\begin{aligned} \langle \mathcal{P}_z \rangle_{\text{can}} = \frac{\epsilon_0 \omega k_z A_0^2}{2} \Big[&\cos^4 \frac{\theta_k}{2} J^2_{m_\gamma - \Lambda}(\kappa\rho) \\ &+ \sin^4 \frac{\theta_k}{2} J^2_{m_\gamma + \Lambda}(\kappa\rho) + \frac{1}{2} \sin^2\theta_k J^2_{m_\gamma}(\kappa\rho) \Big], \end{aligned}$$

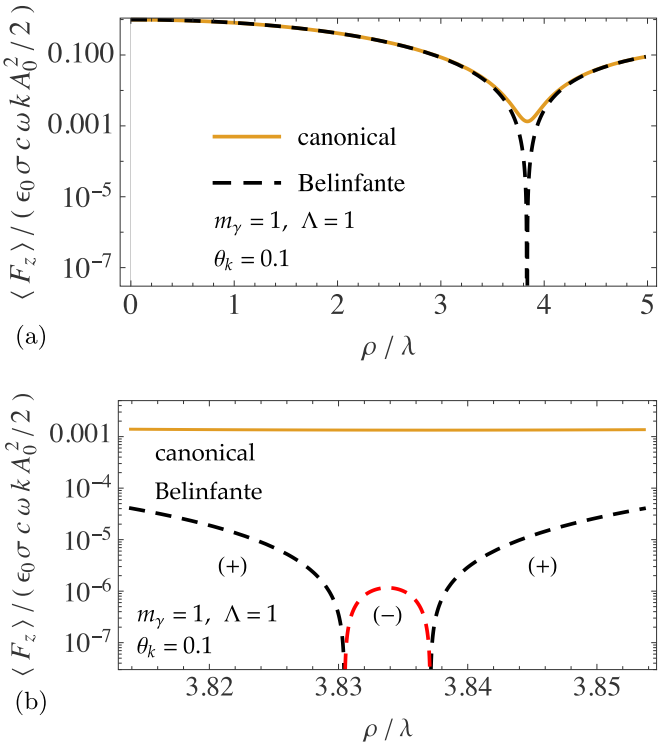

FIG. 5. Force from a twisted light beam on a small dielectric particle at distance ρ from the photon's vortex line for parameters indicated on the plots. (a) gives a broad view, and (b) gives a detailed view. The canonical expression (solid gold line) and Poynting vector expression (dashed black line for positive values, dashed red line for negative values) give similar results except in regions near force minima. Note especially the red dashed curve in (b), where the Belinfante force becomes negative, i.e., points opposite the propagation direction of the beam.

$$\langle \mathcal{P}_z \rangle_{\rm Bel} = \frac{\epsilon_0 \omega k A_0^2}{2} \times \left[\cos^4 \frac{\theta_k}{2} J^2_{m_\gamma - \Lambda}(\kappa\rho) - \sin^4 \frac{\theta_k}{2} J^2_{m_\gamma + \Lambda}(\kappa\rho) \right]. \tag{21}$$

A test object of cross section σ absorbing this momentum density feels a force $\langle F_z \rangle = \sigma c \langle \mathcal{P}_z \rangle$.

The momentum expressions are paraxially the same and are very close numerically over broad regions. Paraxially, the states have $\sigma_z = \Lambda$. However, in the full expressions $\langle \mathcal{P}_z \rangle_{\rm can}$ can never be negative for these modes, while $\langle \mathcal{P}_z \rangle_{\rm Bel}$ is negative at and near radii ρ where coefficient of the usually dominant $\cos^4(\theta_k/2)$ term becomes zero.

Figure 5 shows, for selected m_γ, Λ, and θ_k, the longitudinal force vs distance from the vortex line for the two cases on a small test particle of cross section σ that fully absorbs the beam that strikes it. The results are nearly the same for long stretches of ρ, but the difference near the force minimum is dramatic. Figure 5(b) focuses on a narrow region to emphasize the difference. The canonical case continues pushing in the propagation direction, but in the Belinfante case the radiation pressure becomes a tractor beam at these locations, that is, it pulls toward the source rather than pushes away.

Summary. The canonical and symmetric, or Belinfante, forms of the electromagnetic energy-momentum tensor give identical results for integrated quantities such as the total momentum and total angular momentum of the field. However, they differ point by point in space, and this matters for calculating the force or torque of an electromagnetic wave on a test object of finite size. One requires light with a structured wave front in order to see the differences, and we have worked out examples using Bessel-Gauss beams of twisted photons. In certain regions the differences are dramatic, including tractor-beam effects—also noticed in Ref. [31]—and counterrotating torques predicted when using forces or torques derived from the symmetric momentum tensor. The dramatic contrasts in the force lie in limited spatial regions and are sensitive to details of the beam preparation. The dramatic torque differences, however, are robust and exist over broad spatial regions and could well be confirmed or denied experimentally using ringlike or end-weighted rotor test objects. Numerical results suggest that the generated spin-rate differences could be observable on micron-sized objects, using available twisted-photon beams.

Acknowledgments. We thank E. Leader for inspiring conversations. A.A. thanks the U.S. Army Research Office for supper under Grant No. W911NF-19-1-0022, and C.E.C. thanks the National Science Foundation (USA) for support under Grant No. PHY-1812326. A.M. thanks the SERB-POWER Fellowship, Department of Science and Technology, Government of India, for support.

[1] A. M. Yao and M. J. Padgett, Adv. Opt. Photonics **3**, 161 (2011).
[2] K. Y. Bliokh and F. Nori, Phys. Rep. **592**, 1 (2015).
[3] M. V. Berry, Eur. J. Phys. **34**, 1337 (2013).
[4] S. Albaladejo, M. I. Marqués, M. Laroche, and J. J. Sáenz, Phys. Rev. Lett. **102**, 113602 (2009).
[5] S. Huard and C. Imbert, Opt. Commun. **24**, 185 (1978).
[6] Z.-L. Wang and X.-S. Chen, Phys. Rev. A **99**, 063832 (2019).
[7] M. Ornigotti and A. Aiello, Opt. Express **22**, 6586 (2014).
[8] A. T. O'Neil, I. MacVicar, L. Allen, and M. J. Padgett, Phys. Rev. Lett. **88**, 053601 (2002).
[9] V. Garcés-Chávez, D. McGloin, M. J. Padgett, W. Dultz, H. Schmitzer, and K. Dholakia, Phys. Rev. Lett. **91**, 093602 (2003).
[10] H. He, M. E. J. Friese, N. R. Heckenberg, and H. Rubinsztein-Dunlop, Phys. Rev. Lett. **75**, 826 (1995).
[11] M. E. J. Friese, J. Enger, H. Rubinsztein-Dunlop, and N. R. Heckenberg, Phys. Rev. A **54**, 1593 (1996).
[12] J. I. Cirac and P. Zoller, Phys. Rev. Lett. **74**, 4091 (1995).
[13] C. T. Schmiegelow, J. Schulz, H. Kaufmann, T. Ruster, U. G. Poschinger, and F. Schmidt-Kaler, Nat. Commun. **7**, 12998 (2016).
[14] F. J. Belinfante, Physica (Amsterdam, Neth.) **7**, 449 (1940).

[15] L. Rosenfeld, Mem. Acad. R. Belg. **18**, 1 (1940).
[16] E. Leader, Phys. Lett. B **756**, 303 (2016).
[17] E. Leader, Phys. Lett. B **779**, 385 (2018).
[18] S. M. Barnett and M. V. Berry, J. Opt. **15**, 125701 (2013).
[19] A. Afanasev, C. E. Carlson, and A. Mukherjee, Phys. Rev. Research **3**, 023097 (2021).
[20] I. P. Ivanov, B. Liu, and P. Zhang, Phys. Rev. A **105**, 013522 (2022).
[21] E. Leader and C. Lorcè, Phys. Rep. **541**, 163 (2014).
[22] J. Jauch and F. Rohrlich, *The Theory of Photons and Electrons: The Relativistic Quantum Field Theory of Charged Particles with Spin One-Half*, 2nd ed., Texts and Monographs in Physics (Springer, Berlin, 1976).
[23] J. D. Bjorken and S. D. Drell, *Relativistic Quantum Fields*, International Series in Pure and Applied Physics (McGraw-Hill, New York, 1965).
[24] A. Afanasev, C. E. Carlson, C. T. Schmiegelow, J. Schulz, F. Schmidt-Kaler, and M. Solyanik, New J. Phys. **20**, 023032 (2018).
[25] E. Urban, N. Glikin, S. Mouradian, K. Krimmel, B. Hemmerling, and H. Haeffner, Phys. Rev. Lett. **123**, 133202 (2019).
[26] T. W. Hansch and A. L. Schawlow, Opt. Commun. **13**, 68 (1975).
[27] J. Jin and D. A. Church, Phys. Rev. Lett. **70**, 3213 (1993).
[28] U. D. Jentschura and V. G. Serbo, Phys. Rev. Lett. **106**, 013001 (2011).
[29] U. Jentschura and V. Serbo, Eur. Phys. J. C **71**, 1571 (2011).
[30] A. Afanasev, C. E. Carlson, and A. Mukherjee, Phys. Rev. A **88**, 033841 (2013).
[31] A. V. Novitsky and D. V. Novitsky, J. Opt. Soc. Am. A **24**, 2844 (2007).